Chinese Chemical Letters 37 (2026) 111592

Contents lists available at ScienceDirect

Chinese Chemical Letters

journal homepage: www.elsevier.com/locate/cclet

Constructing highly ion conducting film *via* 3D composite skeleton for dendrite-free lithium metal batteries

Xianzhun Huang[1], Yinlin Luo[1], Bangzhuang Xue, Weiwei Ping*, Hongfa Xiang*

Department of Materials Science and Engineering, Hefei University of Technology, Hefei 230009, China

ARTICLE INFO

Article history:
Received 13 May 2025
Revised 6 July 2025
Accepted 15 July 2025
Available online 22 July 2025

Keywords:
Composite electrolyte films
Dendrite-free
Phase-inversion
3D skeleton
Solid-state li metal batteries

ABSTRACT

Composite solid electrolytes are the most promising candidates for next-generation commercial electrolytes in Li metal batteries. However, the inevitable layered-structure caused by the agglomeration or sedimentation severely impairs the stability and ion conductivity. In this work, by using the phase-inversion within 20 s, we successfully uniformly dispersed $Li_{6.5}La_3Zr_{1.5}Ta_{0.5}O_{12}$ (LLZTO) nano-powders into cellulose acetate, generating a highly conductive and stable 3D composite skeleton film with the thickness of 50 μm. Due to the high heating/cooling rate of 10^4 °C/min, the ultrafast high-temperature sintering (UHS) enables the LLZTO powders with high crystallinity and a size of ~500 nm. Filling the PEGDA polymer, the resulting composite electrolyte films exhibit an ion conductivity of 1.2 mS/cm, nearly 6 times that of the electrolyte film without LLZTO. The composite electrolyte films exhibit excellent stability with Li metal, resulting in a reversible cycling over 2200 h at 0.2 mA/cm^2. Using $LiFePO_4$ and Li metal, the full cell shows a high capacity retention of 99.6 % after 200 cycles and a high rate performance of 1 C. Pairing with NCM811, the cell stable cycles over 110 cycles with a Coulombic efficiency of 99.2 %. This work provides a novel strategy for designing high-performance composite solid electrolytes and paves the way for developing practical SSLMBs with enhanced safety, high energy density, and long cycle life.

© 2026 Published by Elsevier B.V. on behalf of Chinese Chemical Society and Institute of Materia Medica, Chinese Academy of Medical Sciences.

Lithium-ion batteries are increasingly used in electric vehicles due to the urgent need for high energy densities and improved safety [1]. Lithium metal, with its high theoretical specific capacity (3860 mAh/g) and low electrochemical potential (−3.04 V), is a promising anode material [2–6]. However, the growth of dendrites on the lithium metal anode causes significant safety hazards and performance risks [7,8]. Solid-state electrolytes, featuring the higher Young's modulus than Li dendrites, offer a potential solution to safely use the lithium metal anodes [9]. However, their application is limited due to poor contact with electrodes and complex fabrication processes [10,11]. Polymer electrolytes exhibit great flexibility and superior wettability with electrodes, although they suffer from low ion conductivity [12–14].

Composite electrolytes, combining inorganic and organic solid electrolytes, show excellent flexibility and contact with electrodes, and are considered the next-generation electrolytes [15–18]. By lowering the glass transition temperature of the polymer matrix, inorganic nanofillers are employed to mix with the polymer electrolytes to enhance the mobility of local polymer chain segments, increasing the lithium-ion conductivity [19–22]. Meanwhile, adding inorganic electrolytes, the composite electrolytes exhibit improved mechanical strength to inhibit the Li dendrite penetrating through, acquiring high safety. $Li_7La_3Zr_2O_{12}$ (LLZO) with high ionic conductivity and wide electrochemical window (0–5 V) is a commonly used active nanofiller in composite electrolytes [23–26]. However, the agglomerate of the LLZO nanofillers and the inevitable two-phase separated layer structure during processing, significantly impair the mechanical strength and ion conductivity of the composite solid electrolyte [27–29]. To circumvent the layered structure, a three-dimensional inorganic electrolyte skeleton was introduced and filled with the polymer electrolytes [1,27]. Due to the brittleness of the 3D inorganic electrolyte skeleton, the cell with composite electrolytes can not assemble under large pressures, resulting in increasing interface resistances and inferior cycling performance [15,30].

In this work, we developed a highly conductive 3D composite skeleton featuring uniform dispersion of LLZTO nano-powders in the cellulose acetate (Figs. 1a and b) [31–33]. By using ultrafast high-temperature sintering [34,35], we prepared Li_2CO_3-free $Li_{6.5}La_3Zr_{1.5}Ta_{0.5}O_{12}$ (LLZTO) nano-powders within 1–3 s from precursors. Sintering at 1100 °C in the glovebox filling argon gas, the

* Corresponding authors.
E-mail addresses: wwping@hfut.edu.cn (W. Ping), hfxiang@hfut.edu.cn (H. Xiang).
[1] These authors contributed equally to this work.

https://doi.org/10.1016/j.cclet.2025.111592
1001-8417/© 2026 Published by Elsevier B.V. on behalf of Chinese Chemical Society and Institute of Materia Medica, Chinese Academy of Medical Sciences.

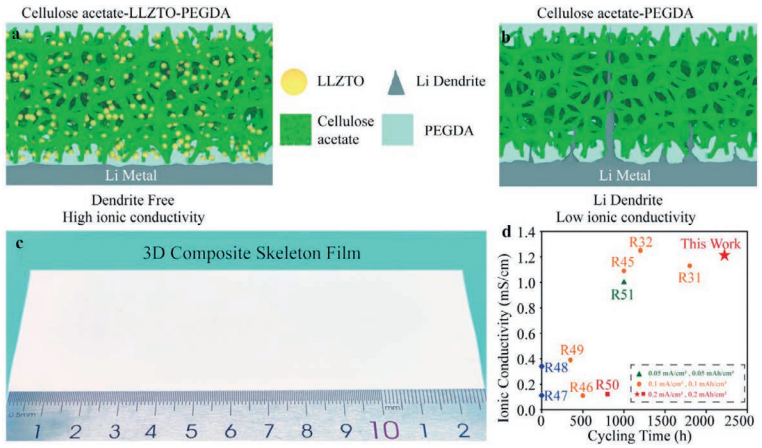


Fig. 1. Schematic diagram of (a) cellulose acetate-LLZTO-PEGDA (CLP) inhibiting Li dendrite penetration compared to (b) cellulose acetate-PEGDA (CAP) film. (c) Digital photos of cellulose acetate-LLZTO (CA-LLZTO) film. (d) Comparison of reported ionic conductivities and cycling performance of symmetric cells using cellulose-based composite electrolyte films [31,32,45–51].

LLZTO powders exhibit high crystallinity. The high cooling rate of 10^4 °C/min can suppress the grain growth, resulting in a powder size of ~500 nm, among the smallest reported powder sizes of the oxide electrolytes [24,36–39]. To prevent the two-phase separation in the drying process, we use phase-inversion to quickly hook the LLZTO nano-powders in the cellulose acetate, resulting in a uniform and mechanically strong 3D composite skeleton without any agglomeration and sedimentation (Fig. 1c and Fig. S1 in Supporting information).

Then, *in-situ* curing polymer electrolytes, like PEGDA, are dipped into the 3D skeleton films to improve their density and facilitate Li-ion transport, increasing the ion conductivity of the composite electrolyte films [18,40–44]. The composite electrolyte films (CLP) show an ion conductivity of 1.2 mS/cm, almost 6 times that of the electrolytes without LLZTO nano-powders (CAP, 0.19 mS/cm), demonstrating the fast Li ion transport pathways contributed by LLZTO nano-powders. The composite electrolyte film enables long-term cycling stability and dendrite suppression in Li-metal batteries. The Li metal anode with this composite electrolyte films (CLP) exhibits excellent reversible and stable long cycle life over 2200 h at 0.2 mA/cm^2 with the duration of 1 h at room temperature, much superior to the reported works (Fig. 1d). Using $LiFePO_4$ cathode and Li metal with composite electrolytes films, the full cell achieves over 200 cycles at 0.5 C with a capacity retention of 99.6 %. Pairing with the high voltage cathode NCM811 and Li metal, the cell cycles 110 times at 0.2 C with a cutoff voltage of 4.2 V. We believe that this approach will provide a new perspective strategy for the application of composite solid electrolyte films in thin-film batteries.

LLZTO electrolytes are easily susceptible to Li_2CO_3 formation upon exposure to air, which were blamed for the decreasing ion conductivity. To preclude the Li_2CO_3 formation, we used the ultrafast high-temperature sintering to fabricate the LLZTO powders in an argon atmosphere. The garnet precursor powders are sprayed from the top of the heater and proceed the crystallization during dropping onto the bottom (Fig. 2a). This sintering time is only 3 s, prohibiting the elements vaporization and grain growth. The grain sizes of the sintered LLZTO powders are controlled to ~500 nm, much smaller than those sintered in the conventional furnace (Figs. S2 and S3 in Supporting information). The UHS sintered LLZTO powders show a planar spacing of 0.288 nm, corresponding to the (420) lattice plane of cubic LLZTO without any Li_2CO_3. The LLZTO powders sintered in the air show a surface layer with a planar spacing of 0.263 nm, corresponding to the (111) lattice plane of Li_2CO_3, which was also confirmed by the SEM results (Figs. 2b and c, Fig. S4 in Supporting information). Profit from the short sintering time of 3 s, the LLZTO powders show a cubic structure without any second-phase (Fig. 2d), suggesting the negligible Li loss.

Then the LLZTO powders with high crystallinity were dispersed in cellulose acetate with *N*,*N*-dimethylformamide (DMF) solvent (Fig. S5 in Supporting information). The mixed solution was cast onto the substrate and then quickly dipped into anhydrous ethanol to proceed the phase-inversion process in 20 s, preventing the Li_2CO_3 formation. Phase-inversion process can well regulate the uniform distribution of the powders in the cellulose acetate bulk, and prevent the layered film structure, which is a common challenge in composite electrolytes fabrication (Fig. S6 in Supporting information). The 3D composite skeleton films are flexible and mechanically strong with a thickness of ~50 μm (Fig. 2e, Figs. S7 and S8 in Supporting information). Uniform elements distribution on the top view and cross-section of the 3D composite skeleton further proves nearly none aggregation or sedimentation of LLZTO powders in the polymer matrix (Figs. 2f and g, Fig. S9 in Supporting information). Benefit for this, the 3D composite skeleton maintains an integrated structure at 60 °C, and is still stable when increasing the temperature to 120 °C. Improving the temperature to 180 °C, close to the melting point of the cellulose acetate (~190 °C), the 3D skeleton films just show a little shrinkage compared to the pure cellulose acetate films, indicating the excellent thermal stability of the 3D composite skeleton films (Fig. 2h).

The PEGDA polymer electrolytes were employed to enhance the density of the 3D composite skeleton. The PEGDA monomers proceed the polymerization in the skeleton induced by HMPP under UV (Figs. S10 and S11 in Supporting information). The resulting in (CLP) films with less solvent of 18.3 wt% show an ion conductivity of 1.2 mS/cm at room temperature, nearly 6 times that of the CAP films, demonstrating the high ion conductivity of the 3D composite skeleton (Fig. 3a and Fig. S12 in Supporting information). With the configuration of SS/composite electrolyte films/SS, we tested the activation energy of Li-ion transport. Similar to the trend of ion conductivities, the CLP films exhibit an activation energy of 0.21 eV, lower than that of CAP films due to the fast Li ion transport pathways provided by the sintered LLZTO powders and interfaces (Fig. 3b). The electrochemical window of the CLP films was assessed *via* linear sweep voltammetry (LSV), where it demonstrates superior stability with oxidation occurring only at 4.5 V, making them suitable for pairing with high-voltage cathodes (Fig. S13 in Supporting information). The lithium transference number (t_{Li^+}) of CLP film is 0.33, higher than the 0.21 of

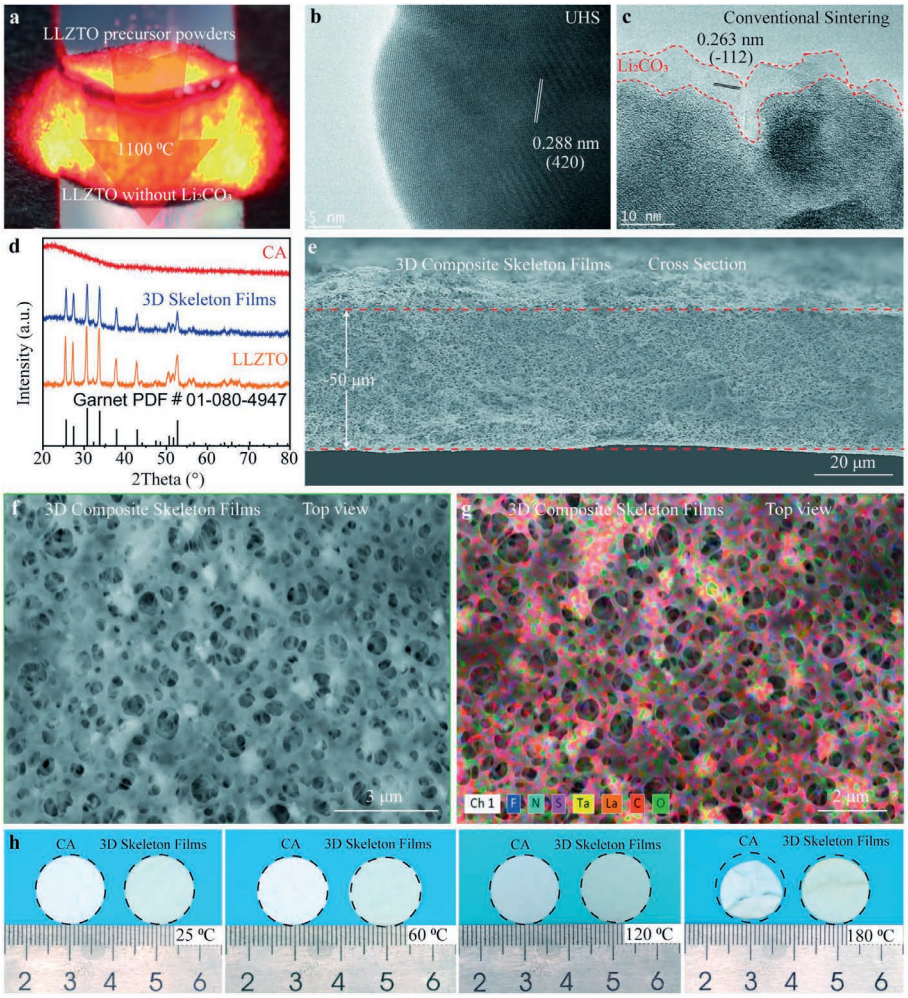


Fig. 2. (a) Digital photos of the UHS sintering process. TEM image of LLZTO particles by (b) UHS and (c) conventional furnace. (d) XRD patterns of CA, 3D composite skeleton films, and UHS-sintered LLZTO powders. (e) SEM image of the cross-section of 3D composite skeleton films. Top view (f) SEM image and (g) EDS mapping of the 3D composite skeleton film. (h) Photographs of the CA film and 3D composite skeleton film after treatment at 25, 60, 120, and 180 °C for 10 min.

CAP films (Fig. S14 in Supporting information). Critical current density was tested at the current densities ranging from 0.1 mA/cm^2 to 1.6 mA/cm^2 with the duration of 30 min. CLP films exhibit a CCD of 1.5 mA/cm^2, higher than the value of CAP films composed of cellulose acetate and polymer electrolytes (0.9 mA/cm^2) (Fig. 3c).

The stability of the composite electrolyte films with Li metal anode is evidenced by cycling the symmetric cell Li/composite electrolyte films/Li at 0.2 mA/cm^2 with a capacity of 0.2 mAh/cm^2 (Fig. 3d). Using the CLP electrolyte films, we achieved excellent cycling performance and a long lifespan over 2200 h. In contrast, using the CAP films, the cell soon fails after 100 h because of short-circuiting caused by Li dendrite penetration. We deposited 4 mAh of lithium metal onto copper foil and examined the cross-sectional morphology of the deposited lithium (Fig. S15 in Supporting information). The lithium metal deposited in the Li/CLP/Li cell exhibits a relatively dense and uniform structure, whereas the lithium deposited in the Li/CAP/Li cell is porous and loosely packed, indicating that the CLP electrolyte facilitates uniform lithium deposition during cycling. In addition, the Li plating/stripping profile of the cell made with the CLP films shows a smaller and more stable voltage hysteresis of 40 mV compared to the CAP films (>100 mV). After 2200 h cycling, the symmetric cell using the CLP showed a slight increase in interface resistance compared to the cell using CAP (short circuit after cycling 100 h), suggesting the durability of the Li anode interface using the CLP films (Fig. S16 in Supporting information). At 60 °C, the Li/CLP/Li cell exhibited stable cycling over 130 h at 0.2 mA/cm^2 with the specific capacity of 0.1 mAh/cm^2 and the Li/CAP/Li cell short-circuited after cycling for 60 h (Fig. S17 in Supporting information). Further increasing the testing temperature to 100 °C, the Li/CLP/Li cell can still stably cycle over 40 h at 0.1 mA/cm^2 with the specific capacity of 0.1 mAh/cm^2 (Fig. S18 in Supporting information). This result demonstrates the potential of the CLP electrolyte film for applications at high temperatures.

In general, the properties of the Li/electrolyte interface in lithium symmetric cells are highly dependent on the lithium deposition behavior, as well as the composition and structure of the solid electrolyte interphase (SEI). In view of this, the micromorphology of Li anodes surface in a Li||Li symmetric cell after cycling for 100 h was observed by SEM (Fig. 3e). 3D composite skeleton can facilitate the ion transporting in the conductive network, resulting in the uniform Li deposition. Benefit for this, Li anodes matching with CLP film display a smooth and dense surface. In comparison, Li anodes pairing with the CAP film exhibit abundant dendritic structures due to the non-uniform Li deposition (Fig. 3f). Coincident with the results of SEM analysis, the surface of Li/CLP/Li cells remained smooth after cycling, with a surface roughness (S_a) of only 1.027 μm, indicating uniform lithium deposition, which is beneficial for enhancing the cycling stabil-

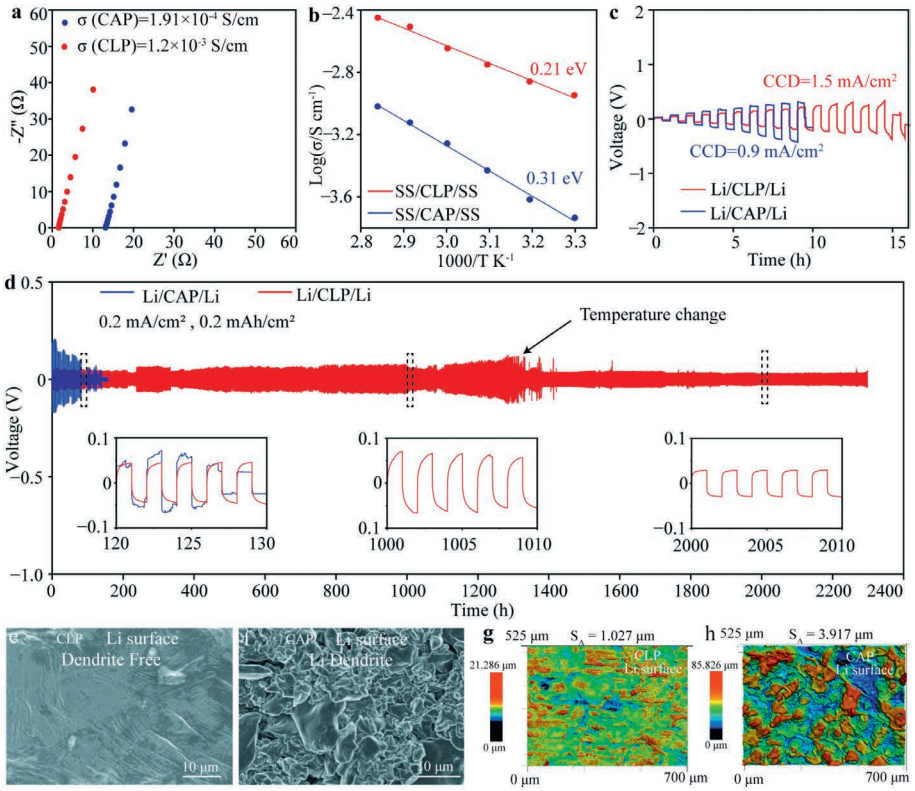


Fig. 3. (a) Nyquist plots and ion conductivity test of SS/CAP/SS and SS/CLP/SS symmetric cells. (b) Activation energy of CLP film fitted by the Arrhenius relationship. (c) Critical current density curves of the symmetric cell Li/CLP/Li and Li/CAP/Li tested at room temperature. (d) Cycling performance of the symmetric cell Li/CLP/Li and Li/CAP/Li at 0.2 mA/cm^2 with the specific capacity of 0.2 mAh/cm^2. SEM images of the lithium metal surface of (e) Li/CLP/Li and (f) Li/CAP/Li cells after 100 h of cycling. 3D morphology reconstruction of cycled Li anodes over 100 h with (g) CLP and (h) CAP film *via* LSM.

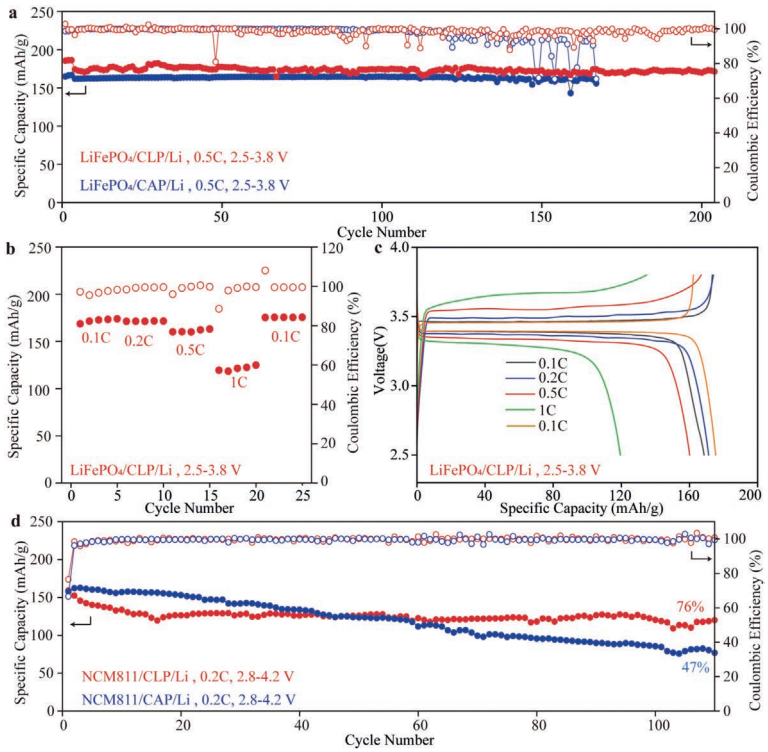


Fig. 4. (a) Galvanostatic cycling of $LiFePO_4$/CLP/Li and $LiFePO_4$/CAP/Li cell at 0.5 C at room temperature. (b) Rate performance and (c) corresponding charge-discharge curves of $LiFePO_4$/CLP/Li cell at room temperature. (d) Galvanostatic cycling of NCM811/CLP/Li and NCM811/CAP/Li cells at 0.2 C at room temperature.

ity of the battery (Fig. 3g). In contrast, the S_a of lithium metal in the Li/CAP/Li cell reached 3.917 μm after cycling, suggesting the formation of a large number of lithium dendrites on the surface (Fig. 3h). To determine the chemical composition of the SEI layer in the composite electrolyte films, the XPS characterization was performed on the Li/electrolyte interface in the cycled symmetric cell (Fig. S19 in Supporting information). A high content of LiF was detected by the Li 1s XPS spectrum of the Li anode matching with CLP films. The higher content of LiF in the F 1s spectrum of the Li surface of Li/CLP/Li cell, along with the lower contents of LiTFSI and $LiPF_6$. Notably, LiF can improve the ion carrier concentration meanwhile impeding electron transport, thereby effectively suppressing lithium dendrite growth and protecting the lithium anode from corrosion [31].

To evaluate the performance of the CLP films in full cell, we use $LiFePO_4$ cathode to couple with the CLP films with Li metal and cycle the cell at 0.1 C for 5 cycles (1 C = 170 mAh/g), followed by increasing the cycling current density to 0.5 C at room temperature (Fig. 4a, Figs. S20 and S21 in Supporting information). The full cell with CLP films shows a higher charge/discharge capacity and lower overpotential than the cell using CAP films. The Li/CLP/$LiFePO_4$ cell runs over 200 cycles with a capacity retention of 99.5 %. The Li-metal battery using CLP films also exhibits outstanding rate performance, delivering discharge capacity of 171.4, 171.3, 160.1, and 118.4 mAh/g at 0.1, 0.2, 0.5, and 1 C respectively (for the second cycle at each rate) (Fig. 4b). When the rate changes from 1 C to 0.1 C, the reversible capacity recovers to 175.5 mAh/g, suggesting excellent reversibility (Fig. 4c). In comparison, the cell using the CAP films only exhibited discharge capacity of 167.7, 166.4, 160, and 142.4 mAh/g at 0.1, 0.2, 0.5 and 1 C respectively (for the second cycle at each rate), and there is an overcharge phenomenon at 1 C (Fig. S22 in Supporting information). When paired with the high-voltage cathode NCM811 together with Li metal, the full cell exhibits a discharge capacity of 159.2 mAh/g with a capacity retention of 74 % after 110 cycles at 0.2 C, significantly higher than the Li/CAP/NCM811 cell (47 %) (Fig. 4d, Figs. S23 and S24 in Supporting information). Impedance spectroscopy further confirms the excellent stability of the anode interface, highlighting the robust performance of the Li/CLP-based electrolyte system during long-term cycling.

In conclusion, we have developed a highly conductive composite electrolyte film based on cellulose acetate for lithium-dendrite-free batteries. LLZTO powders sintered by ultrafast high-temperature sintering method show high crystallinity with a powder size of ~500 nm. By conducting the phase-inversion within 30 s, the LLZTO-cellulose acetate films show uniform structure without any aggregation or sedimentation within the bulk, facilitating the Li-ion transporting. By filling the PEGDA cross-linked polymer, the CLP composite electrolyte films with less solvent (18.3 wt%) exhibit a high ion conductivity of 1.2 mS/cm, 6 times that of the CAP films (0.19 mS/cm) without LLZTO powder additives. Benefiting from the uniform distribution of LLZTO powders, the CLP films exhibit excellent stability with Li metal. The Li/CLP/Li symmetric cell maintains consistent lithium deposition/stripping and cycles stably over 2200 h at a current density of 0.2 mA/cm^2 with a specific capacity of 0.2 mAh/cm^2, much superior to the reported works. These CLP films also show high performance in full cells. The $LiFePO_4$/CLP/Li full cell maintains over 200 cycles at 0.5 C with a high capacity retention of 99.5 % and exhibits a high rate of 1 C. Using CLP composite electrolyte films to pair with high voltage cathode of NCM811 and Li metal, the full cell stably cycles over 110 cycles with a Coulombic efficiency of 99.2 %. This study introduces a promising strategy for the development of novel cellulose-based electrolyte films in advanced energy storage systems.

CRediT authorship contribution statement

Xianzhun Huang: Methodology, Investigation, Data curation, Conceptualization. **Yinlin Luo:** Visualization, Investigation, Data curation, Conceptualization. **Bangzhuang Xue:** Investigation, Data curation, Conceptualization. **Weiwei Ping:** Writing – review & editing, Writing – original draft, Supervision, Methodology, Investigation. **Hongfa Xiang:** Writing – review & editing, Writing – original draft, Supervision.

Acknowledgments

This work was financially supported by the National Natural Science Foundation of China (No. 52202227) and the Fundamental Research Funds for the Central Universities of China (No. JZ2025HGTB0209). We acknowledge the support of the Instrumental Analysis Center of Hefei University of Technology.

Supplementary materials

Supplementary material associated with this article can be found, in the online version, at doi:10.1016/j.cclet.2025.111592.

References

[1] Y. Zheng, Y. Yao, J. Ou, et al., Chem. Soc. Rev. 49 (2020) 8790–8839.
[2] X. He, K. Zhang, Z. Zhu, et al., Chem. Soc. Rev. 53 (2024) 9–24.
[3] Z. Zhang, W.Q. Han, Nano Micro Lett. 16 (2023) 24.
[4] C.Z. Sun, L. Zhang, X. Wang, J. Li, Sci. Adv. 4 (2018) eaau1971.
[5] M. Gandolfo, M. Longo, T. Diemant, et al., J. Energy Chem. 107 (2025) 221–232.
[6] Z.Z. Dong, J.H. Zhang, L. Zhu, et al., Chin. Chem. Lett. 36 (2025) 109773.
[7] F. Sun, C. Yang, I. Manke, et al., Mater. Today 38 (2020) 7–9.
[8] C. Yan, X.B. Cheng, Y. Tian, et al., Adv. Mater. 30 (2018) 1707629.
[9] R. Chen, Q. Li, X. Yu, et al., Chem. Rev. 120 (2019) 6820–6877.
[10] H. Huo, J. Gao, N. Zhao, et al., Nat. Commun. 12 (2021) 176.
[11] O. Sheng, C. Jin, T. Yang, et al., Energy Environ. Sci. 16 (2023) 2804–2824.
[12] H. Liu, Y. Liao, C. Leung, et al., Adv. Energy Mater. 15 (2024) 2402795.
[13] Z. Song, F. Chen, M. Martinez-Ibañez, et al., Nat. Commun. 14 (2023) 4884.
[14] D. Li, X. Liu, Y. Li, et al., Adv. Energy Mater. 14 (2024) 2402929.
[15] X. Zhang, S. Cheng, C. Fu, et al., Nano Micro Lett. 17 (2024) 2150–5551.
[16] Y. Guo, X. Qu, Z. Li, et al., Chin. Chem. Lett. 35 (2024) 108482.
[17] H. Xiang, N. Deng, L. Gao, et al., Chin. Chem. Lett. 35 (2024) 109182.
[18] P. Li, J. Hao, S. He, et al., Nat. Commun. 16 (2025) 3727.
[19] X. Lu, Y. Wang, X. Xu, et al., Adv. Energy Mater. 13 (2023) 2301746.
[20] Q. Ma, S. Fu, A.J. Wu, et al., Adv. Energy Mater. 13 (2023) 2203892.
[21] M. Ge, X. Zhou, Y. Qin, et al., Chin. Chem. Lett. 33 (2022) 3894–3898.
[22] L.Z. Fan, H. He, C.W. Nan, Nat. Rev. Mater. 6 (2021) 1003–1019.
[23] H. Liang, L. Wang, A. Wang, et al., Nano Micro Lett. 15 (2023) 42.
[24] C. Wang, K. Fu, S.P. Kammampata, et al., Chem. Rev. 120 (2020) 4257–4300.
[25] D. Li, H. Liu, C. Wang, et al., Adv. Funct. Mater. 34 (2024) 2315555.
[26] C. Wang, W. Li, D. Li, et al., ACS Nano 18 (2024) 32175–32185.
[27] L. Chen, X. Huang, R. Ma, et al., Energy Storage Mater. 65 (2024) 103140.
[28] G. Wang, Y. Liang, H. Liu, et al., Interdiscip. Mater. 1 (2022) 434–444.
[29] X. Zhao, C. Wang, X. Fan, et al., InfoMat 7 (2025) e70012.
[30] X. Zhang, M.V.M. Nitou, W. Li, et al., Chin. Chem. Lett. 34 (2023) 108245.
[31] D. Wang, H. Xie, Q. Liu, et al., Angew. Chem. Int. Ed. 62 (2023) e202302767.
[32] R. Wang, W. Dong, Z. Song, et al., Adv. Funct. Mater. 34 (2024) 2402461.
[33] H. Jeon, H.A. Hoang, D. Kim, J. Energy Chem. 74 (2022) 128–139.
[34] C. Wang, W. Ping, Q. Bai, et al., Science 368 (2020) 521–526.
[35] W. Ping, C. Wang, R. Wang, et al., Sci. Adv. 6 (2020) eabc8641.
[36] W. Wang, M. Jia, Z. Bi, X. Guo, Adv. Funct. Mater. 35 (2025) 2419182.
[37] Y. Wang, P. Yuan, X.X. Liu, et al., Adv. Funct. Mater. 34 (2024) 2405060.
[38] X. Xie, P. Zhang, X. Li, et al., J. Am. Chem. Soc. 146 (2024) 5940–5951.
[39] J. Zhu, S. He, H. Tian, et al., Adv. Funct. Mater. 33 (2023) 2301165.
[40] Q. Liu, L. Wang, X. He, Adv. Energy Mater. 13 (2023) 2300798.
[41] S. Zou, Y. Yang, J. Wang, et al., Energy Environ. Sci. 17 (2024) 4426–4460.
[42] K. He, S.H. Cheng, J. Hu, et al., Angew. Chem. Int. Ed. 60 (2021) 12116–12123.
[43] X. Li, C. Yi, W. Hu, et al., Chin. Chem. Lett. 36 (2025) 110215.
[44] S. Zhao, J. Lu, B. Sheng, et al., Chin. Chem. Lett. 36 (2025) 110008.
[45] J. Li, Z. Hu, S. Zhang, et al., Nat. Sustain. 7 (2024) 1481–1491.
[46] C. Wang, D. Huang, S. Li;, et al., Nano Lett. 20 (2020) 7397–7404.
[47] H. Xie, C. Yang, K. Fu, et al., Adv. Energy Mater. 8 (2018) 1703474.
[48] C. Yang, Q. Wu, W. Xie, et al., Nature 598 (2021) 590–596.
[49] J. Yang, Z. Cao, Y. Chen;, et al., ACS Nano 17 (2023) 19903–19913.
[50] K. Zhou, M. Zhang, X. Zhang, et al., Chem. Eng. J. 464 (2023) 142537.
[51] H. Zhang, S. Wang, A. Wang, et al., Appl. Surf. Sci. 593 (2022) 153411.